A PON Monitoring Scheme for Online Fault Detection and Localization

Xuan Zhang and Ning Ning

Abstract—We propose and experimentally demonstrate an on-line PON monitoring scheme that can simultaneously achieve the objectives of fault detection and localization. Fault detection and localization share the same transmitter module and perform in sequence. Based on a simple algorithm, one or several fiber Bragg gratings with different central reflection wavelengths are allocated to each end-user for fault detection. A large number of wavelength combinations are generated by several fiber Bragg gratings with different center wavelengths, and are finally identified in the time domain, which is very suitable for fault detection of large-capacity and high-density PON. An additional module is added before the power splitter/combiner to ensure the online troubleshooting. The model equation is established to locate the fault using two un-modulated broadband light sources. The calculated results of the fault localization method show a good agreement with the OTDR measurement results. The proposed scheme provides an integrated online troubleshooting solution for the detection and localization of PON link faults.

Index Terms—Fault detection, Fault localization, Monitoring system, Passive optical network (PON).

I. INTRODUCTION

THE data-intensive applications, such as high-definition video-on-demand, online video streaming services, cloud computing/storage services and high-speed internet access, have led to a sharp increase demand for bandwidth [1]–[3]. Specifically, the consumer bandwidth in residential areas and businesses is growing at a rate of nearly 50% per year [4], [5]. To satisfy such a quick growth, passive optical network (PON) has been widely deployed across the globe since it offers high bandwidth, very long reach, and easier deployment [6]–[10]. For instance, GPON is already the dominant technology choice in North America and Europe. EPON has been successfully deployed in Eastern Asia, such as China, Japan, and South Korea. At the same time, China–the world's largest fiber to the home (FTTH) market–also embarked on a large-scale deployment using a mix of EPON and GPON [11]. With the successful

deployment of PONs on a large scale worldwide, PONs face significant challenges to provide a certain level of reliability without exceeding the budget constraints of cost-sensitive access networks [12]. The loss of significantly higher traffic volumes that may be caused by fiber link failures has attracted more and more attention [13], [14]. Furthermore, network operators also urgently need a PON monitoring system to improve troubleshooting efficiency and reduce customer dissatisfaction and complaints.

It is known that optical-time-domain reflectometry (OTDR) techniques are widely used in point-to-point (P2P) networks. However, it has major limitations in tree topology or point-to-multipoint (P2MP) network like PONs [15], [16]. In P2MP networks the OTDR trace at the central office (CO) is aggregation of the backscattered and reflected powers from all the network branches [17]. It is difficult for the CO network manager to distinguish the events in one branch from those in others. Due to the failure of OTDR in P2MP networks, many PON monitoring schemes have been widely presented to improve the service reliability [15]–[19]. Mainstream PON monitoring schemes usually focus on centralized monitoring, and most of them can take into account factors such as cost, difficulty of implementation, and effectiveness. When one or several drop fiber (DF) links fail, these existing schemes can effectively identify which DF in the network is faulty. This process is often referred to as fault detection and is the first objective of any PON monitoring system [18]. The period coding (PC) scheme may be considered as one of the earliest proposed schemes for fault detection, which has the characteristics of simple structure and low cost [20]. A 2-D optical frequency hopping/periodic coding scheme (OFH/PC) is proposed to reduce the excessive multiple-customers interference probability (MCIP) of the PC scheme [21]. However, the OFH/PC scheme makes the encoder structure complicated and the cost increases. That is, encoders for the OFH/PC scheme require more fiber Bragg gratings (FBGs) with different central reflection wavelength (CRW) and more fiber patch cords. The self-match based on polling scheme balances MCIP, encoder structure and cost to a certain extent [22]. Unfortunately, since this scheme adopts the principle of link-by-link identification, it reduces the efficiency of fault detection. The second objective is fault localization but it is rarely considered in existing schemes. Normally, OTDR is used to find exact location of a fault on the faulty branch. Nevertheless, OTDR and the original fault detection system are relatively independent and are not conducive to system integration. It is worth noting that, for the
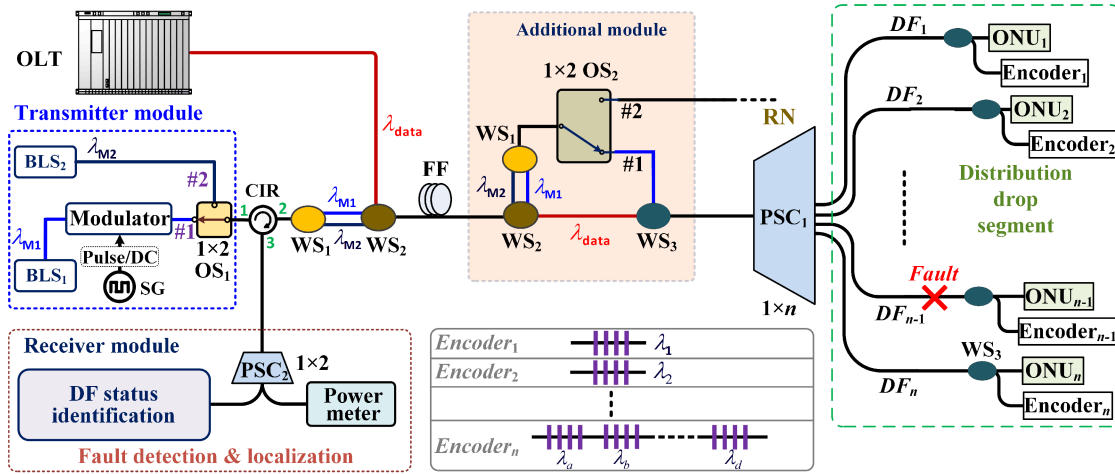
Fig. 1.   Schematic diagram of the proposed scheme.

second objective (i.e., fault localization) alone, without the use of OTDR, the transmission-reflection-analysis (TRA) method has been proposed to guarantee an appropriate level of long-reach PON reliability and performance [23]. The TRA method is based on the unique relationship between the optical powers transmitted and backscattered for a given loss location, and has superior detection speed and simple system configuration compared to other conventional approaches.

In this paper, we propose and experimentally demonstrate a PON monitoring scheme for fault detection and localization. With the same transmitter module, fault detection and localization can be completed in one system at the same time. For the objective of fault detection, each DF link configures a corresponding number of FBGs with different CRWs according to the proposed algorithm. The reflected light signal of each DF link is identified in the time domain after being converted into an electrical signal. It is worth pointing out that the core devices used in the encoders of the proposed scheme and many other schemes are FBGs, but they are quite different in the principle of encoding and decoding (or working principle). In the modified optical code division multiplexing scheme, the encoders contain 5 different structures [24]. The fifth encoder structure (MBG encoder) consist of a series of discrete FBGs at the same CRW but with different reflection intensities and physical locations. This approach uses optical encoders that generate pseudo-orthogonal codes to identify each end-user form the other. In the PC scheme, encoders use a pair of FBGs with the same CRW and different reflectivity forming a cavity to generate periods codes [20]. The cavity length inserted between FBGs fixes cavity length and differentiates the codes. The status on individual DF link can be discernable at the CO due to the near orthogonality of the codes generated. In the wavelength-to-time mapping scheme, each encoder contains only one FBG with the same CRW and different spectral bandwidth. The technique employs the wavelength-to-time mapping effect of broadband short pulses in a highly dispersive medium. The spectral bandwidth of the corresponding encoder is deduced by measuring the temporal width of the reflected pulse [25]. For the objective of fault localization, two unmodulated broadband light sources (BLSs) with different center wavelengths are sequentially injected into

the network, and the location of the breakpoint is solved through the established model equation. Note that two wavelengths continuous-wave (CW) approach can be used to localize the major fault in the ring-based long-reach optical access networks [26]. The shared BLS can effectively reduce the influence of FBG on temperature sensitivity, thus ensuring the performance of fault detection. An additional module is added before the remote node (RN), which can ensure online troubleshooting. That is, the troubleshooting of one DF link would not affect the normal communication of other DF links. In addition, we also calculate the wavelength combination of each DF link in a PON with 64 end-users and investigate the measurable length points of the model equation established.

II. PRINCIPLE AND DESIGN

Fig. 1 illustrates the principle of the proposed PON monitoring scheme. The transmitter module consists of two BLSs, a modulator and a 1×2 optical switch (OS). The 1×2 OS_1 located in the transmitter module is placed on channel #1 by default. The OS at the RN has the drawback to require power supply in the field, which may be not consistent with the principle of PONs. However, the use of the OS also provides the possibility of automatic switching between fault detection and fault localization. Note that automation is one of many required features in a PON monitoring scheme [18]. The monitoring signal emitted by the BLS_1 is modulated by a modulator driven by a signal generator (SG). That is, the pulse drive signal is triggered and modulates the broadband signal passing through the modulator. The monitoring signal (i.e., λ_{M1} or λ_{M2}) and the traffic data (i.e., λ_{data}) from the optical line terminal (OLT) are coupled through a wavelength selector (WS) and sent into the feeder fiber (FF). The additional module is mainly composed of three WSs and a 1×2 OS. The wavelength channels corresponding to WS_1, WS_2 and WS_3 are $\{\lambda_{M1}, \lambda_{M2}\}$, $\{\lambda_{M1}, \lambda_{M2}, \lambda_{data}\}$ and $\{\lambda_{M1}, \lambda_{data}\}$, respectively. The monitoring signal of λ_{M1} and the data signal are separated by the WS_2 and recombined by the WS_3. Note that the 1×2 OS_2 is now placed on channel #1. The modulated λ_{M1} signal is divided into n subpulses by the power splitter/combiner (PSC) at the RN and distributed to

each DF link. The encoder at the front of each optical network unit (ONU) can extract and reflect spectrum part corresponding to the FBGs used. The components in the encoder have good compatibility with optical fibers. Meanwhile, simple structure and lower cost can increase acceptance by network operators. Then, the reflected monitoring signals are sent into the receiver module via a circulator (CIR). Finally, the corresponding signals are sent to the network recognition algorithm for the network status evaluation. Status of each DF link can be obtained by analyzing the combination of wavelengths generated. When the fault DF link is successfully identified, the fault detection process has been completed. Then, the OS_2 needs to be switched to channel #2 and connected to the corresponding faulty DF link. At this time, OS_1 in the transmitter module is still placed on channel #1. Note that fault detection can only complete the binary decision (i.e., normal or fault) of the DF link status. When a break occurs at any position on the DF link, the fault detection can only show that the DF link is faulty but not the specific location of the break.

In the above fault detection process, each encoder can generate FBG reflection spectrum with one or several different CRWs. However, the FBG(s) used on each encoder needs to follow a specific algorithm. This algorithm not only guarantees system performance, such as a small MCIP, but also minimizes the total number of FBGs used. Here, we take Monte Carlo simulations with 64 randomly assigned located customers in a PON with circular coverage area of 6000 m^2 at 10^5 times iteration to calculate the MCIP. In this calculation, the pulse width of the monitoring signal used in both the PC scheme and the proposed scheme is 1 ns, and the code weight in the PC scheme is set to 4. The MCIP of the PC scheme and the proposed scheme are roughly 0.7878 and 0.0046, respectively. For a PON with n end-users, the required number of different CRWs satisfy $K = 1 + \log_2 n$. For instance, in a PON with 64 end-users, 7 kinds (i.e., $K = 7$) of FBGs with different CRWs can effectively monitor all DF links, i.e., $\lambda_1, \lambda_2, \lambda_3, \lambda_4, \lambda_5, \lambda_6, \lambda_7$. Note that different CRWs of FBGs are distinguished by the various subscripts (i.e., 1, 2, 3, …) of λ. We assume that the different wavelength combinations, labeled by subscripts, produced by each encoder collectively form a set. Also, the subscripts of the CRW in each set are arranged in ascending order. The subscript sets (i.e., t_1 t_2...t_w, $w \leq m$) of CRWs corresponding to the yth DF link ($y = 1, 2, …, n$) can be calculated as

$$y = \sum_{j=1}^{w} [C(K, j) - C(K - t_j, w + 1 - j)] \quad (1)$$

where $C(p, q)$ means that q objects are selected from a set of p objects to produce subsets without ordering. Here, we define $C(p, q) = 0$ ($p < q$). The maximum value of m depends on n. For instance, m equal to 4 can support 64 end-users network monitoring. Specifically, the number of FBGs with different CRWs for the 1st~7th, 8th~28th, 29th~63rd and 64th end-users are 1, 2, 3 and 4, respectively. Eq. (1) describes the correspondence between the DF link number and the subscripts. Obviously, w corresponds to the number of FBG(s) used on each DF link. According to the rule of the set subscripts arranged in ascending order, t_w represents the maximum value in a set of

subscripts combinations. The relationship between y and w in Eq. (1) satisfies: $\sum_{r=1}^{w} C(K, r - 1) \leq y \leq \sum_{r=1}^{w} C(K, r)$. For a PON with 64 end-users (i.e., $n = 64$), the combination of $t_1 = 2$ and $t_2 = 4$ (i.e., $w = 2$) can make y equal to 15. That is, the monitoring wavelength combination of the 15th DF link is $\{\lambda_2, \lambda_4\}$.

Recall that fault detection is only the first objective of any PON monitoring system. Fault localization (i.e., the second objective) is also required to further improve troubleshooting efficiency. When the break occurs in one or several DF links and is successfully identified, the established model equation is employed to calculate the location of the break. Suppose a break occurs at x_b on a DF link and its return loss is RL_b [dB]. For the input monitoring signal, it would produce attenuation, reflection and scattering as transmitted in the network system. Then, the total received backscattered/reflected power (P_{TR}) [mW] of the proposed monitoring scheme in Fig. 1 can be written as

$$P_{TR(i)} = P_{in(i)} \left\{ 10^{\left(-\frac{DIR}{10}\right)} + 10^{\left(-\frac{RL_{WS1} + RL_{WS2}}{10}\right)} \right.$$

$$+ RAY_i(L_{FF}) \cdot 10^{\left(-\frac{IL_{WS1i} + IL_{WS2i}}{5}\right)}$$

$$+ T_i^2(L_{FF}) \cdot 10^{\left(-\frac{IL_{WS1i} + IL_{WS2i}}{5}\right)}$$

$$\cdot \left[10^{\left(-\frac{RL_{WS1} + RL_{WS2}}{10}\right)} \right.$$

$$\left. + 10^{\left(-\frac{IL_{WS1i} + IL_{WS2i}}{5}\right)} \cdot 10^{\left(-\frac{RL_{OS2}}{10}\right)} \right]$$

$$+ [RAY_i(L_{FF} + x_b) - RAY_i(L_{FF})]$$

$$\cdot 10^{\left(-\frac{2IL_{WS1i} + 2IL_{WS2i} + IL_{OS2i} + \alpha_C}{5}\right)}$$

$$+ T_i^2(L_{FF} + x_b) \cdot 10^{\left(-\frac{2IL_{WS1i} + 2IL_{WS2i} + IL_{OS2i} + \alpha_C}{5}\right)}$$

$$\left. \cdot 10^{\left(-\frac{RL_b}{10}\right)} \right\} \cdot 10^{\left(-\frac{IL_{CIRi} + IL_{PSC2i}}{10}\right)} \quad (2)$$

$P_{in(i)}$ is the input power before injection into port 1 of the CIR. $T_i(x)$ is the fiber transmission coefficient and can be written as: $T_i(x) = exp(-\alpha_i x)$, where α_i [km^{-1}] is the fiber attenuation coefficient. DIR [dB] is the directivity of the CIR that indicates power transmitted directly from port 1 to port 3. IL_{WS}, IL_{OS}, IL_{CIR} and IL_{PSC} are the insertion loss (in dB) of the WS, 1×2 OS_2, CIR, and 1×2 PSC, respectively. α_C represent the connection loss between the channel #2 of the OS_2 and the corresponding fault DF link. RL_{WS} and RL_{OS} are the return loss (in dB) of the WS and OS, respectively. $RAY_i(x)$ is the Rayleigh backscattered power coefficient that can be expressed as [26]

$$RAY_i(x) = S_i \cdot \alpha_{Si} \cdot [1 - \exp(-2\alpha_i x)]/2\alpha_i \quad (3)$$

α_{si} is the scattering coefficient due to the Rayleigh scattering. S_i is the capture coefficient and x is the length of the fiber segment. Since the proposed PON monitoring system uses two BLSs with different center wavelengths, and the parameters such as fiber transmission coefficient and Rayleigh backscattered power coefficient are wavelength dependent, the subscript i ($i = 1$ for BLS$_1$ and $i = 2$ for BLS$_2$) is added to distinguish the values
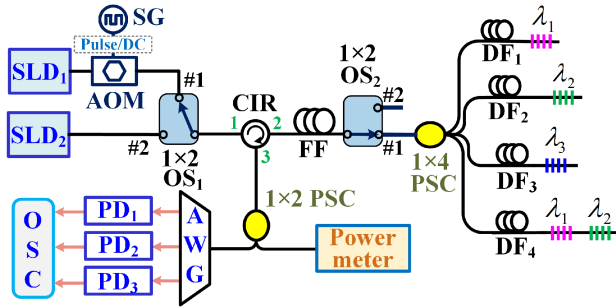
Fig. 2.   Experimental setup.

Fig. 3.   Experimental results of fault detection: (a) All four DF links are normal; (b) a break occurs in the DF$_4$ link.

TABLE I
COMPARISON BETWEEN THE CALCULATED RESULTS AND OTDR
MEASURED RESULTS

Calculated result	OTDR measured result
1026m	1034m
2027m	2036m
2996m	3002m

under different BLSs. It should be noted that the insertion loss is wavelength sensitive but the return loss is insensitive [26].

Two equations can be obtained by sequentially injecting dual BLSs with different center wavelengths. Except for x_b and RL_b, all other parameters are known or measurable. Therefore, two equations with two unknown variables can be solved. With the same transmitter module, we can use the above-established model equation to complete fault localization. In [26], the authors have employed dual unmodulated CW in the ring-based long-reach optical access networks and established an overdetermined equation system to solve the problem of fault localization. In the proposed scheme, two unknowns form a system of equations. In the case where the attenuation coefficients of the two fibers do not satisfy a specific relationship, a numerical solution with high accuracy can also be obtained by the least squares method.

III. EXPERIMENTAL DEMONSTRATION

The experiment is demonstrated in a simplified 1×4 PON system, and the experimental setup is illustrated in Fig. 2. Due to equipment containment, two superluminescent diodes (SLDs) with center wavelengths of 1550 nm and 1310 nm are used as the monitoring signal. The CRWs of the three FBGs with a 3-dB reflection bandwidth of about 0.1 nm and a reflectivity of about 95% are $\lambda_1 = 1548.5$ nm, $\lambda_2 = 1550.1$ nm, $\lambda_3 = 1551.7$ nm, respectively. An acoustic optical modulator (AOM) is used to generate the rectangular monitoring pulse with duration of $1\mu s$ and a pulse repetition rate of 10 kHz. For the fault detection process, an optical amplifier is also added between the AOM and CIR to compensate the power loss. A 20.363 km-long standard single-mode fiber is used as the FF. Four encoders constructed by FBGs with different CRWs locate at the end of each DF link. For fault detection, two mechanical 1×2 OS$_1$ and OS$_2$ are placed on channel #1. Note that in the process of fault detection, the drive source of the AOM is a pulse signal. That is, the broadband optical signal output by SLD$_1$ is modulated into a periodic pulse monitoring signal. The total received signals are demutiplexed by an arrayed waveguide grating (AWG). After the photoelectric conversion by the photodetectors (PDs), the waveform traces are acquired by the real-time oscillography (OSC) Agilent Infiniium 54833A.

The monitoring signals corresponding to DF$_1$, DF$_2$, DF$_3$ and DF$_4$ are $\{\lambda_1\}$, $\{\lambda_2\}$, $\{\lambda_3\}$ and $\{\lambda_1, \lambda_2\}$, respectively. Fig. 3(a) indicates that all DF links are in a normal status. A severely
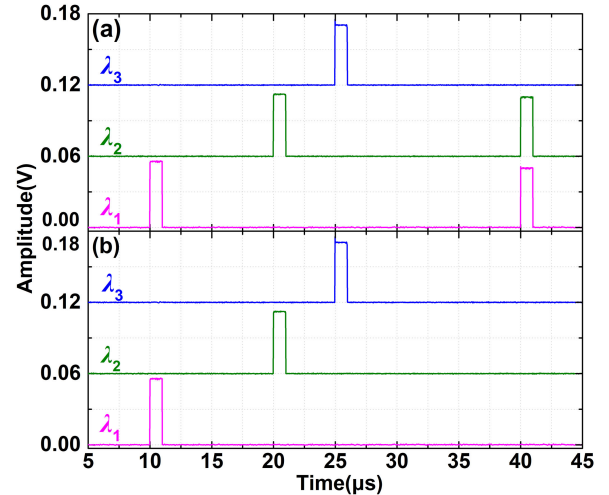
attenuated level signal indicates that the corresponding DF link has a break. Fig. 3(b) shows that DF$_4$ is broken, and the corresponding signal levels at the same time domain position are missing.

After the corresponding fault DF link (i.e., DF$_4$) is identified, we can further locate the breakpoint on the DF using the established model equation as described above. Note that the driving source of the AOM is DC signal at this time. That is, the broadband optical signal output by SLD$_1$ is unmodulated. For the fault localization, the 1×2 OS$_2$ with return loss of 55 dB needs to be switched to channel #2. Recall that the insertion loss is wavelength sensitive while the return loss is not. The insertion loss of the OS$_2$ at 1550 nm and 1310 nm are 0.8 dB (i.e., $i = 1$) and 0.68 dB (i.e., $i = 2$), respectively. To save the power budget, the optical power meter is directly connected to the port 3 of the CIR. The insertion loss of CIR with DIR of 60 dB at 1550 nm and 1310 nm are 2.21 dB and 2.02 dB, respectively. The input power injected into the port 1 of CIR corresponding to 1550 nm and 1310 nm are 3.47 mW and 6.09 mW, respectively. For comparison purposes, three breakpoint locations are also measured by a commercial OTDR (Agilent E6003A Mini-OTDR). The calculated results obtained by the established model equation and measured results by OTDR are listed in Table I. Here, we use the same input power in the three calculation measurements. The two total received power values (i.e., $P_{TR(1)}$ and $P_{TR(2)}$) generated by two SLDs are substituted into Eq. (2) with an $S_i \cdot \alpha_{si}$ of 0.00022 ($i = 1$) and 0.00048 ($i = 2$), α_i of 0.0437 km^{-1} ($i = 1$) and 0.0759 km^{-1} ($i = 2$). $S \cdot \alpha_s$ can be calculated by connecting an optical isolator to the end of the FF with known length.
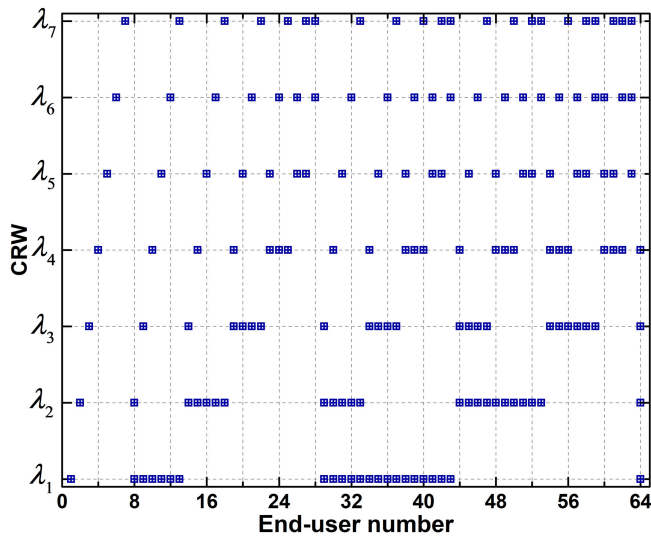
Fig. 4.   Wavelength combination for a PON with 64 end-users.

IV. Calculation and Analysis

A. Wavelength Combination of Fault Detection

In the process of fault detection, each DF link needs to be configured with a unique wavelength combination. In these wavelength combinations, except for the single wavelength of the first K end-users, the others all contain two or more. Multiple FBGs with different CRWs in the encoder are connected in cascade mode. Since the monitoring wavelengths generated by different FBGs in each wavelength combination travel the same distance in the network, they have the same time domain position on different wavelength channels. When the reflected level signal of the wavelength combination at the same time domain position is missing together, it indicates that the corresponding DF link is broken. It should be pointed out that even if the DF link lengths of different end-users are the same, the proposed scheme can effectively distinguish each other. Specifically, the same DF link length causes the wavelength combination signal level to be the same in the time domain, however, each wavelength combination contains different wavelengths and is identified on different wavelength channels. Obviously, compared to the identification on a single channel, it can reduce the probability of overlapping between reflected level signals. Therefore, the fault detection technology is very suitable in a high-density PON. Note that the receiver module can accurately identify the faulty DF link depends on it knowing the wavelength combination of each DF link in advance. In this proposed scheme, a large number of wavelength combinations can be obtained from a few FBGs with different CRWs. In Fig. 4, we use Eq. (1) to calculate the wavelength combination for each DF link in a PON with 64 end-users. For such a PON, 7 FBGs with different CRWs (i.e., $\lambda_1, \lambda_2, \lambda_3, \lambda_4, \lambda_5, \lambda_6, \lambda_7$) are required in the encoders to generate 64 wavelength combinations. For instance, the wavelength combinations of the 1st, 8th, 32nd and 64th ports are $\{\lambda_1\}$, $\{\lambda_1, \lambda_2\}$, $\{\lambda_1, \lambda_2, \lambda_6\}$ and $\{\lambda_1, \lambda_2, \lambda_3, \lambda_4\}$, respectively. Note that the number of FBGs in the encoders of other end-users is less than 4 except for the 4 FBGs used in the encoder of the 64th
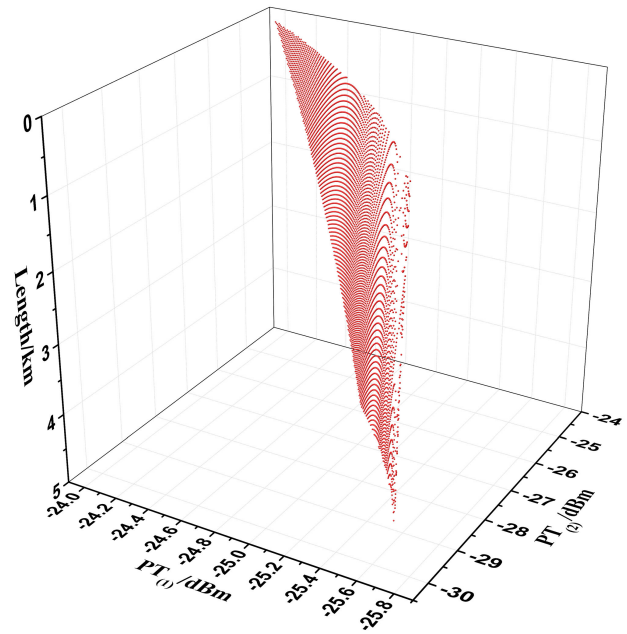

Fig. 5.   Possible measurable length points in the range of DF link within 5 km.

end-user. Obviously, the fault detection technology is also very suitable in a large-capacity PON.

B. Calculation Accuracy of Fault Localization

In the proposed scheme, two unmodulated BLSs with different center wavelengths are injected into the network sequentially to generate a set of equations. Recall that except for x_b and RL_b, all other parameters are known. When eliminating RL_b in the equations, we can get a transcendental equation about x_b. Note that the fiber attenuation coefficient is wavelength-dependent. When the fiber attenuation coefficient under different BLS meets a certain relationship (e.g., $\alpha_1 = \alpha_2$ or $\alpha_1 = \alpha_2/2$), the transcendental equation about x_b can be solved analytically. In other cases, such as $\alpha_1 = 0.19$ dB/km and $\alpha_2 = 0.33$ dB/km, the equation may be solved numerically by the least square method. However, the setting of calculation accuracy plays an important role in obtaining accurate numerical solutions. A numerical solution with good accuracy indicates that when x_b and RL_b solved by the transcendental equation are substituted into Eq. (2), the $P_{TR(1)}$ and $P_{TR(2)}$ values calculated should be consistent with the original values. That is, with a given computational precision, the values on both sides of Eq. (2) can remain equal. When the calculated values of $P_{TR(1)}$ and $P_{TR(2)}$ are different from the original values, the corresponding solutions x_b and RL_b may be inaccurate. Therefore, some inaccurate values should be removed from the solution set. Fig. 5 illustrates the solutions in the range of 0~5 km, which corresponds to the possible measurable length points in the distribution segment. In this calculation, the measurement accuracy of the optical power meter is set to 0.01 dB. Note that when these length solutions and the corresponding return loss values are substituted into Eq. (2) again, the values on both sides of the equal sign remain the same. In most instances, the reflectivity of the fiber end is less than 1%,

corresponding to the return loss of 20 dB [27]. Here, the return loss of the fiber break ranges from 20 dB to 60 dB. The further calculation results show that the maximum difference between any two adjacent length points does not exceed 8 m.

V. Conclusion

We have proposed and experimentally demonstrated a PON monitoring scheme that can simultaneously complete fault detection and localization. Fault detection in this proposed scheme uses the FBGs with different CRWs to identify the fault in the time domain. Fault localization method uses the established model equation to calculate the break location, which can achieve a good accuracy. The wavelength combinations corresponding to a PON with 64 end-users are calculated using Eq. (1). The possible measurement points with a length of 0∼5 km and a return loss of 20∼60 dB are also investigated. The calculation results show that the established model equation can be solved by the least square method with good accuracy. The proposed scheme can provide a promising solution for the integration of fault detection and localization.

References

[1] M. S. Erkilinc et al., "Comparison of low complexity coherent receivers for UDWDM-PONs (λ-to-the-User)," *J. Lightw. Technol.*, vol. 36, no. 16, pp. 3453–3464, Aug. 2018.
[2] J. Hecht, "The bandwidth bottleneck that is throttling the internet," *Nature*, vol. 536, no. 7615, pp. 139–142, Aug. 2016.
[3] K. Bourg, S. Ten, R. Whitman, J. Jensen, and V. Diaz, "The evolution of outside plant architectures driven by network convergence and new PON technologies," in *Proc. Opt. Fiber Commun. Conf.*, Los Angeles, CA, USA, 2017, pp. 1–3.
[4] P. Miguelez, "What applications are driving higher capacity in access?," in *Proc. Opt. Fiber Commun. Conf.*, San Diego, CA, USA, 2018, pp. 1–3.
[5] J. George, "Start thinking about 3 to 30 gbps by 2030!," *Broadband properties*, pp. 42–47, Mar. 2022. [Online]. Available: http://www.broadbandproperties.com/2006issues/sep06issues/george_sep.pdf
[6] N. Suzuki et al., "100 Gb/s to 1 Tb/s based coherent passive optical network technology," *J. Lightw. Technol.*, vol. 36, no. 8, pp. 1485–1491, Apr. 2018.
[7] D. Nesset, "PON roadmap," *J. Opt. Commun. Netw.*, vol. 9, no. 1, pp. A71–A76, Jan. 2017.
[8] P. P. Iannone et al., "Increasing TDM rates for access systems beyond NG-PON2," *J. Lightw. Technol.*, vol. 34, no. 6, pp. 1545–1550, Mar. 2016.
[9] T. Horvath et al., "Passive optical networks progress: A tutorial," *Electronics*, vol. 9, no. 7, Jul. 2020, Art. no. 1081.
[10] C. DeSanti et al., "Super-PON: An evolution for access networks," *J. Opt. Commun. Netw.*, vol. 12, no. 10, pp. D66–D77, Oct. 2020.
[11] J. Salgado et al., "New FTTH-based technologies and applications," *A White Paper by the Deployment & Operations Committee*, Mar. 2022. [Online]. Available: http://citeseerx.ist.psu.edu/viewdoc/download?doi=10.1.1.683.3349&rep=rep1&type=pdf
[12] N. Ghazisaidi, M. Scheutzow, and M. Maier, "Survivability analysis of next-generation passive optical networks and fiber-wireless access networks," *IEEE Trans. Reliab.*, vol. 60, no. 2, pp. 479–492, Jun. 2011.
[13] M. M. Rad, H. A. Fathallah, and L. A. Rusch, "Fiber fault PON monitoring using optical coding: Effects of customer geographic distribution," *IEEE Trans. Commun.*, vol. 58, no. 4, pp. 1172–1181, Apr. 2010.
[14] V. Sangeetha et al., "Optical fiber cable fault localization in FTTH network using OTDR," *Int. J. Res. Comput. Appl. Robot.*, vol. 3, no. 3, pp. 205–212, Mar. 2015.
[15] X. Zhang and X. H. Sun, "Optical pulse width modulation based TDM-PON monitoring with asymmetric loop in ONUs," *Sci. Rep.*, vol. 8, no. 1, Mar. 2018, Art. no. 4472.
[16] N. F. Naim et al., "Real-time monitoring in passive optical networks using a superluminescent LED with uniform and phase-shifted fiber Bragg gratings," *J. Opt. Commun. Netw.*, vol. 5, no. 12, pp. 1425–1430, Dec. 2013.
[17] M. M. Rad, K. Fouli, H. A. Fathallah, L. A. Rusch, and M. Maier, "Passive optical network monitoring: Challenges and requirements," *IEEE Commun. Mag.*, vol. 49, no. 2, pp. S45–S52, Feb. 2011.
[18] M. A. Esmail and H. Fathallah, "Physical layer monitoring techniques for TDM-passive optical networks: A survey," *IEEE Commun. Surv. Tut.*, vol. 15, no. 2, pp. 943–958, Jan. 2013.
[19] X. Zhang, T. Yang, and X. Jia, "PON monitoring scheme using wavelength-bandwidth identification of a single fiber Bragg grating," *IEEE Photon. Technol. Lett.*, vol. 33, no. 8, pp. 387–390, Apr. 2021.
[20] H. Fathallah, M. M. Rad, and L. A. Rusch, "PON monitoring: Periodic encoders with low capital and operational cost," *IEEE Photon. Technol. Lett.*, vol. 20, no. 24, pp. 2039–2041, Dec. 2008.
[21] X. Zhou, F. Zhang, and X. Sun, "Centralized PON monitoring scheme based on optical coding," *IEEE Photon. Technol. Lett.*, vol. 25, no. 9, pp. 795–797, May 2013.
[22] X. Zhang et al., "Self-match based on polling scheme for passive optical network monitoring," *Opt. Commun.*, vol. 417, no. 15, pp. 19–23, Feb. 2018.
[23] M. Cen et al., "Advanced transmission-reflection-analysis (TRA) system for long-reach passive optical network monitoring," in *Proc. 17th Int. Conf. Transparent Opt. Netw.*, Budapest, Hungary, 2015, pp. 1–4.
[24] H. Fathallah and L. A. Rusch, "Code-division multiplexing for in-service out-of-band monitoring of live FTTH-PONs," *J. Opt. Netw.*, vol. 6, no. 7, pp. 819–829, Jul. 2007.
[25] M. P. Fernández, L. A. Bulus Rossini, and P. A. Costanzo Caso, "PON monitoring technique using Single-FBG encoders and Wavelength-to-Time mapping," *IEEE Photon. Technol. Lett.*, vol. 31, no. 21, pp. 1745–1748, Nov. 2019.
[26] M. Cen et al., "Advanced fault-monitoring scheme for ring-based long-reach optical access networks," *J. Lightw. Technol.*, vol. 35, no. 10, pp. 1876–1886, May 2017.
[27] Z. H. Luo et al., "Fiber-end antireflection method for ultra-weak fiber Bragg grating sensing systems," *Meas. Sci. Technol.*, vol. 32, no. 5, Mar. 2021, Art. no. 055109.